An experimental study on the upper part-load elliptical vortex instability in a Francis turbine

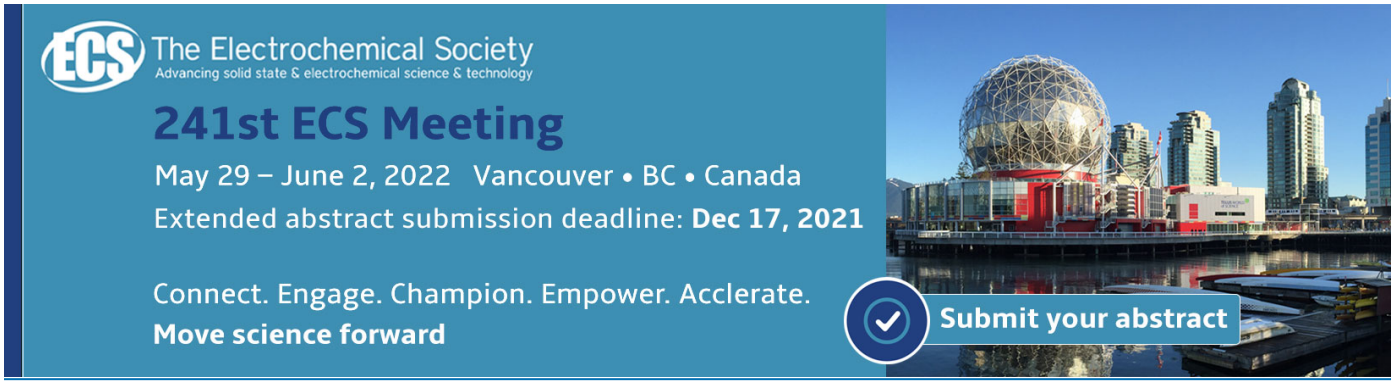

An experimental study on the upper part-load elliptical vortex instability in a Francis turbine

Ali Amini[a], Elena Vagnoni[a], Arthur Favrel[b], Kazuhiko Yamaishi[c], Andres Müller[a], François Avellan[a]

[a] Laboratory for Hydraulic Machines, École Polytechnique Fédérale de Lausanne, Lausanne, Switzerland

[b] Waseda Research Institute for Science and Engineering, Waseda University, Tokyo, Japan

[c] Nippon Koei Co., Ltd., Power & Digital Business Unit, Sukagawa, 962-8508, Japan

Corresponding author's email address: ali.amini@epfl.ch

Abstract:

This paper presents preliminary results of an experimental study on the occurrence and development of the upper part-load instability in a reduced-scale Francis turbine. The study includes draft tube pressure measurements, high-speed flow visualization, and particle image velocimetry. Our results reveal that for an operating point within the range of the upper part-load instability (70 to 85 % of the nominal discharge), the vortex rope has a circular cross section in non-cavitating conditions, which is preserved even after the appearance of cavitation within the vortex core. It is only below a certain cavitation number that the vortex cross section turns into an ellipse, which is associated with an abrupt increase in the pressure fluctuations with a distinct peak in the frequency domain. A further decrease in the cavitation number results in a constant decrease in the activated frequency while the amplitude of these oscillations experience a rise followed by a quick drop. Phase-averaged velocity fields show that the occurrence and development of cavitation within the vortex rope result in a more diffused distribution of the angular momentum. The instantaneous velocity fields, on the other hand, reveal that the elliptical vortex has various states with either diffused or concentrated velocity distributions, which makes the use of the averaged velocity field for this point less relevant.

Introduction

Francis turbines operating in part-load conditions develop a precessing vortex rope within the draft tube with a frequency (f_{rope}) corresponding to 0.2 to 0.4 of the runner rotational frequency. Particularly, in the higher part load operation range, i.e. 70 to 85 % of the nominal discharge, this phenomenon might be accompanied by large-amplitude pressure fluctuations with a distinct frequency peak (f_{upper}) in the range of 2–4 times the runner rotational frequency [1, 2, 3]. The occurrence of this instability leads to severe vibrations in the hydraulic circuit, which affect the performance of the machine. It is therefore crucial to develop a better understanding of this phenomenon and explain how different parameters influence this instability mode.

This upper part-load instability is usually associated with an elliptical-shaped vortex rope. Koutnik et al. [4] attribute the high-frequency pulsations to the self-rotation of the elliptical vortex rope, which develops an asymmetrical pressure distribution around itself. This hypothesis has been evidenced by Kirschner et al. [5], too. In addition to the self-rotation of the elliptical cross section, Nicolet et al. [3] also bring up the possibility of a breathing pattern in the evolution of the cavitation volume with time and the draft tube pressure. This phenomenon has been recently studied by Favrel et al. [6] who use two

cameras to obtain a more realistic estimation of the cavitation volume in the draft tube. They also highlight the occurrence of intermittent collapses, which lead to the formation of two distinct cavities on the two sides of the elliptical cross section. Despite the existing literature on the topic, the causes of this instability along with its impacts on the flow structures are not yet well known. The present paper aims at developing a better insight into the initiation mechanism of the upper part-load instability as well as its effects on the velocity field. To this end, high-speed visualizations, pressure measurements and velocimetry techniques have been deployed. First, the effect of cavitation number on the shape of the cavitating vortex rope is investigated. This is followed by the analysis of the pressure measurements in the time and frequency domains. In the end, the velocimetry results for cavitating and non-cavitating vortex ropes are presented and discussed.

Experimental Setup

The measurements are carried out on a reduced-scale model of a Francis turbine installed on platform 3 of EPFL LMH. The tested turbine has a specific speed equal to 0.33, which is defined by:

$$\nu = \frac{\omega Q^{1/2}}{\pi^{1/2}(2E)^{3/4}}$$

The reduced-scale model includes the upstream inlet pipe, the spiral case, the runner with a reference diameter $D = 0.35$ m, and the draft tube consisting of the cone, the elbow and the diffuser. The operating conditions of this test model are defined based the IEC International Standard by the speed coefficient ($n_{11} = ND/\sqrt{H}$) and the discharge coefficient ($Q_{11} = Q/D^2\sqrt{H}$). In our experiments, the rotational speed and the head were set to 849 rpm and 21 m, respectively. At the Best Efficiency Point (BEP), Q_{11} is equal to 0.69 $m^{0.5}s^{-1}$. Pressure fluctuations in the draft tube are measured by three flush-mounted piezo-resistive pressure sensors with a sampling frequency set to 1 kHz. For the high-speed flow visualizations, a Photron (Fastcam Mini AX 200) camera is utilized at a recording rate of 2,000 frames per second. To obtain the velocity fields in the draft tube, Particle Image Velocimetry (PIV) method has been implemented by means of a 200-mJ double-pulsed laser, a CCD camera and fluorescent particles, which allow for measurements in the presence of cavitation. A side view of the reduced-scaled model and the draft tube is shown in Figure 1. The position of the pressure sensors as well as the lower and upper PIV planes are also depicted in this figure.

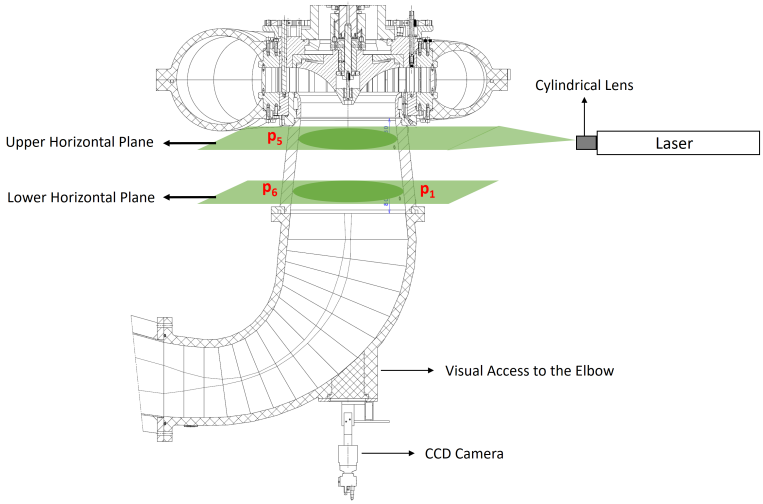

Figure 1: PIV setup and the position of the pressure sensors and the measurement planes in the draft tube

For each operating condition, we acquire 10,000 PIV images. The pressure in the draft tube is recorded synchronously with the PIV trigger pulses. This information is used later to define the relative position of each PIV instant between two successive pressure minima that are induced periodically by the passage of the precessing vortex. The instantaneous velocity fields are then averaged based on their phase on the precession cycle.

Results and discussion

The effect of reducing the cavitation number on the state of the cavitating vortex rope in the draft tube is illustrated in Figure 2. The results correspond to an operating point with nominal head and rotational speed and $Q_{11}/Q_{11,BEP} = 0.84$. At the higher cavitation number of $\sigma = 0.16$, the vortex rope possesses a circular cross section. It is enough to slightly reduce the cavitation number to $\sigma = 0.14$ to initiate the instability. At this cavitation number, the vortex rope cross section takes an elliptical shape and emits high-amplitudes noise at frequencies higher than f_{rope}. This trend continues as the cavitation number is further reduced. At the lower values of σ (i.e. 0.08 and 0.06), the vortex rope loses its coherent shape and shows chaotic behavior with intermittent collapses and recoveries.

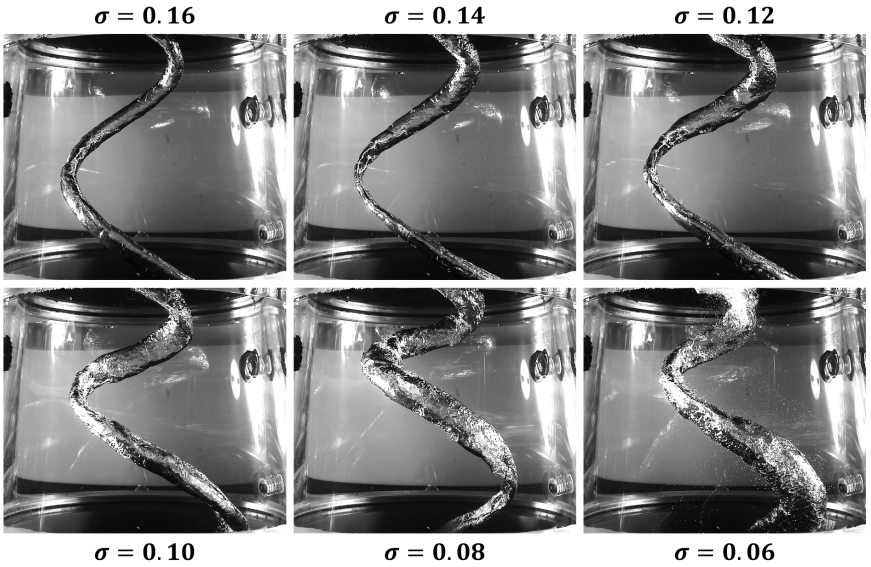

Figure 2: Effect of cavitation number on the state of the cavitating vortex rope at $Q_{11} = 0.58$.

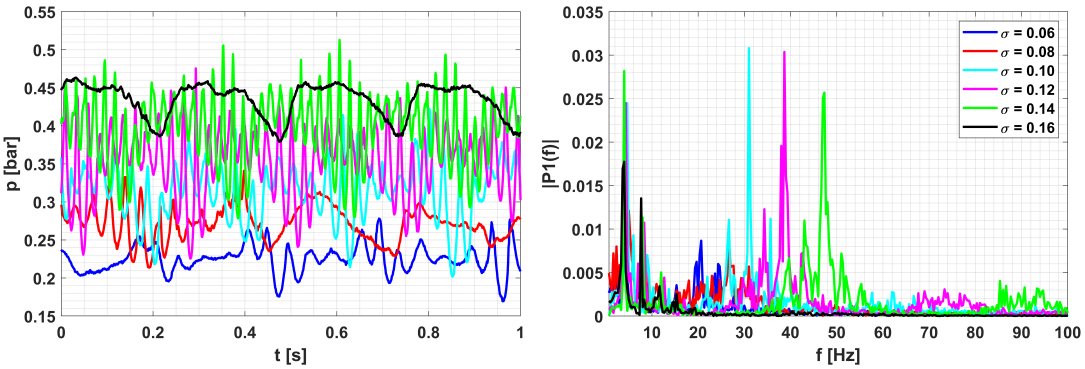

Figure 3: Effect of cavitation number on pressure variations in the draft tube and its frequency content.

The variation of the cone pressure is shown in Figure 3 (left), which is measured at position p_1 over a period of 1 s for the same flow condition and cavitation numbers as in Figure 2. As is clear, at $\sigma = 0.16$, the upper part-load instability is not yet activated and the pressure signal corresponds to the periodic passage of the vortex by the sensor position. However, at $\sigma = 0.14$, the pressure signal presents a different pattern and has a much richer content. As the instability initiates at this point, high-amplitude oscillations at f_{upper} modulate with the precession frequency. The measured signals at $\sigma = 0.12$ and 0.10 are very similar to that of $\sigma = 0.14$. However, at the lower values of the cavitation number, the vortex starts to lose its coherent shape due to the increased amount of cavitation in the cone, and consequently, the modulation is undermined.

The power spectrum of the measured pressure signals for the same flow conditions is illustrated in Figure 3 (right). The peaks that are closely placed at around 4 Hz and 8 Hz correspond to f_{rope} and its first harmonic. At the higher value of $\sigma = 0.16$, no other distinct peaks are observed. However, the initiation of the instability at $\sigma = 0.14$ is associated with the appearance of an outstanding peak at about 48 Hz. As the cavitation number is further reduced to 0.12 and 0.10, f_{upper} decreases constantly while the magnitude of the peak increases considerably. At lower values of cavitation number, f_{upper} continues to decrease further, however, the amplitude of the fluctuations at f_{upper} reduces drastically. A deeper look at the plot reveals the existence of side peaks next to the higher frequency peaks at $f_{upper} \pm f_{rope}$, which is in line with the previous studies [4, 6].

The reported behavior of the oscillation amplitudes is in contrast to a previous study [3], which reported an almost constantly decreasing trend for the amplitude of the fluctuations at f_{upper}. The authors believe that the occurrence and development of the upper part-load instability depends strongly on the cavitation volume in the draft tube. For the higher values of σ, the amount of cavitation is not enough to lead to such high-amplitude oscillations. Depending on the operating condition, there might be a critical cavitation number, for which the circular vortex turns into an elliptical shape. This gives rise to pressure fluctuations at f_{upper}, most probably due to the self-rotation of the vortex, as suggested in [3, 5, 6]. Once the instability is initiated, a further increase in the cavitating volume increases the compressibility of the flow and leads to higher-amplitude pressure fluctuations. This could also be related to a breathing mechanism [3], which gets more pronounced as the vapor volume increases in the draft tube. Finally, for extremely high amounts of cavitating volumes, the flow loses its coherence due to intermittent collapses, which leads to the division of the energy content in a wider range of frequencies.

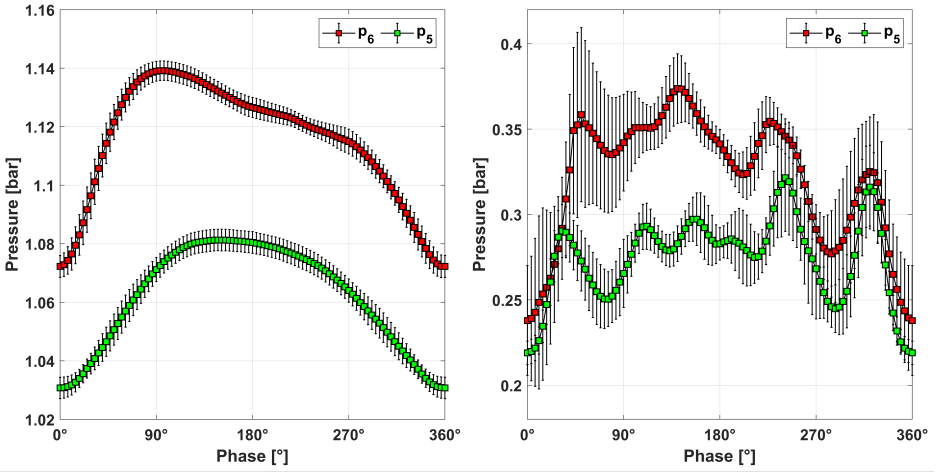

Figure 4: Phase-averaged pressure signals over the precession cycle. Left: non-cavitating conditions with a stable precessing vortex, Right: cavitating vortex rope at $\sigma = 0.09$ with upper part-load instability activated.

PIV measurements were performed for the nominal conditions in terms of head and rotational velocity and for a slightly lower discharge value ($Q_{11}/Q_{11,BEP} = 0.80$) compared to the previous results, in order to limit the amount of cavitation it the draft tube and ensure an optimal visual access to the measurement planes. The variation of the draft tube pressure is depicted in Figure 4, in which the pressure is measured at the locations of the upper (p_5) and lower (p_6) laser planes for the non-cavitating precessing vortex (left) and the cavitating vortex rope with the upper part-load instability initiated (right). These pressure signals have been phase-averaged on the precession cycle based on the min-to-min location over 1000 seconds of PIV acquisition for each operating point. As is clear in Figure 4, the activation of the upper part-load instability leads to inter-period fluctuations within the main precession cycle and increases the standard deviation of the signals significantly. It is also inferred from Figure 4 (right) that the amplitude of the fluctuations is much higher at p_6, which is located at a lower position in the draft tube.

The results presented in Figure 4 (left) imply that for the non-cavitating precessing vortex, the flow structure should change significantly at the upper and lower measurement planes. Close to the turbine outlet (p_5), the pressure follows an almost symmetrical evolution in terms of the rise and decrease times. At the lower plane (p_6), however, this symmetry breaks and the pressure rises much faster than it takes for it to decrease back to minimum (3/4 of the cycle). This interesting behavior could be explained by the average velocity fields that are shown in Figure 5. At the upper plane (left), the vortex core is more concentrated and possesses a relatively axisymmetric pattern compared to the lower plane (right). Given that the precession direction is counter-clockwise, the vortex at the lower plane is preceded by an area with high tangential velocity compared to the upper plane. This accelerated flow contributes to a local depression that arrives at the sensor location before the vortex passage and can explain why the pressure decrease phase takes a longer potion of the cycle in the lower plane.

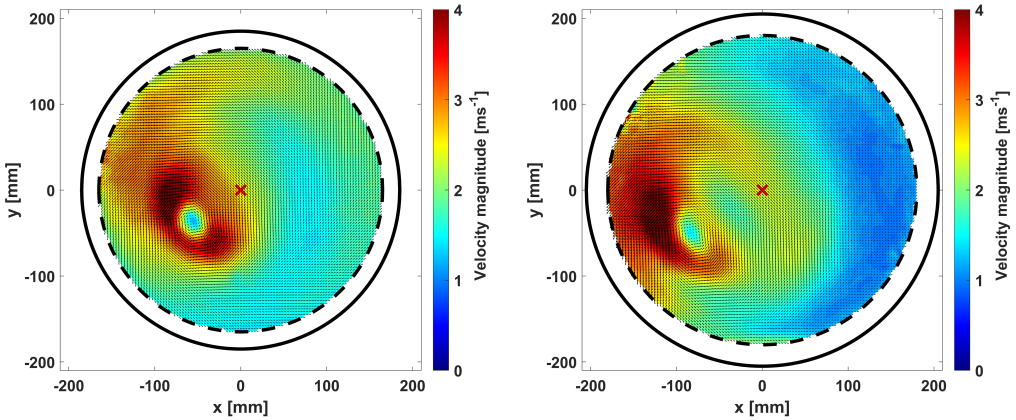

Figure 5: PIV contours in the upper and the lower planes of measurement

Presented in Figure 6 are the phase-averaged velocity fields measured at the upper plane for three values of cavitation number. The image at left corresponds to the non-cavitating flow while the contours at the middle and right are obtained for cavitating vortices with $\sigma = 0.20$ and $\sigma = 0.09$, respectively. The cavitating vortex in the middle has a circular cross section while the one at right possesses an elliptical cross section. As a cavitating vortex partly blocks the PIV images and consequently the obtained velocity field, the vortex centers are not clear in the middle and right contours.

It is perceived from the contours presented in Figure 6 that the occurrence of cavitation within the core of the precessing vortex (comparison of the left and middle images) may first lead to a slight increase in the magnitude of the circumferential velocity. As the center of the vortex is occupied by vapor, whose angular momentum could be neglected compared to the liquid phase, the remaining swirl at the turbine outlet has to be distributed over a lower surface area. It is harder to compare the result at $\sigma = 0.09$ with the two other points, as the cavitating vortex is quite large and blocks a considerable amount of the view.

It may still be inferred that the velocity field is more diffused for the lowest value of cavitation number. Although the maximum of tangential velocity adjacent to the vortex core is diminished, it seems to have slightly increased at the larger radii.

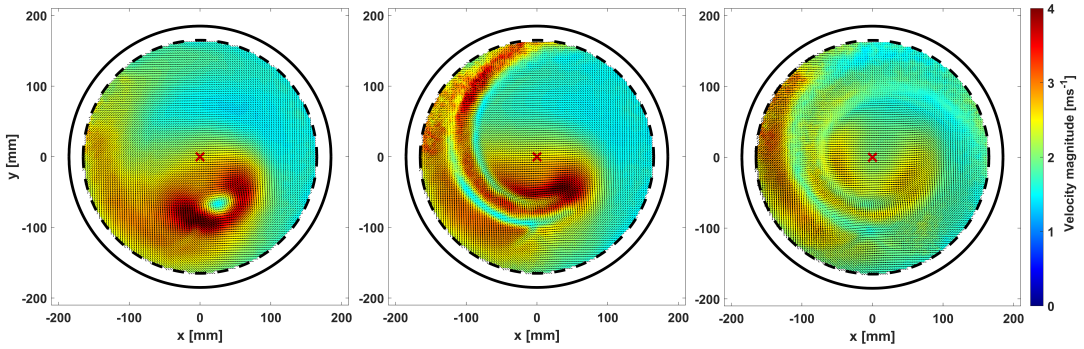

Figure 6: Phase-averaged velocity fields for non-cavitating (left) and cavitating vortices at $\sigma = 0.20$ (middle) and at $\sigma = 0.09$ (right).

In order to achieve a better insight into the flow in the presence of cavitation, some PIV moments along with their instantaneous velocity fields are shown in Figure 7. The left picture corresponds to $\sigma = 0.20$ with circular vortex shape. The two other instants are associated with an elliptical vortex at $\sigma = 0.09$ where both pictures have been taken at the same phase of the precession cycle. All the pictures related to the circular vortex correspond more or less to the same shape as presented in Figure 7. However, this does not hold for the elliptical vortex, as its state is not fully described only by the precession phase. As it is clear in Figure 7 (middle), at the moments when the elliptical vortex rope occupies a smaller volume, the velocity field surrounding it resembles much to the one of the circular vortex (the left contour). This includes the magnitude and the distribution pattern. On the contrary, when the elliptical vortex holds a larger volume in the plane of measurement, which could be due to a breathing effect, the velocity field alters in a way that the magnitude of the circumferential velocity decreases close to the vortex core and increases at farther positions. These results suggest that the phased-averaged velocities on the precession cycle do not represent the flow adequately. Further investigations are still ongoing in this regard.

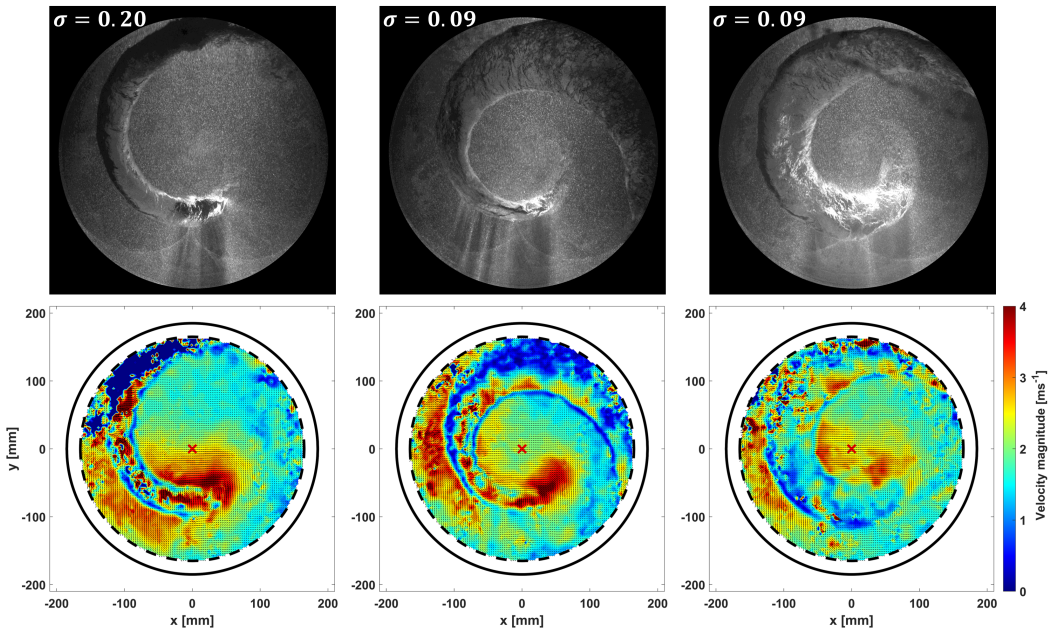

Figure 7: Instantaneous PIV moments and the corresponding velocity fields with the cavitating vortex rope.

Conclusion

In this paper, we investigated the upper part-load instability phenomenon in a reduced-scale Francis turbine model. Our results have shown that the upper part-load instability does not occur above a certain value of the cavitation number for a specific operating condition. The vortex rope first holds a circular shape and it is only below a critical cavitation number that the circular cross section turns into an elliptical one associated with high-amplitude pressure fluctuations at f_{upper}. A further decrease in σ results in the reduction of the excited frequency while the amplitude of the fluctuations increases. Once the cavitation volume reaches a relatively high volume, intermittent collapses begin to occur in the draft tube, which in turn affect the coherence of the vortex and reduce the amplitude of the fluctuations at f_{upper}. The PIV measurements performed in the presence of the cavitating vortex rope have revealed that the velocity field around the elliptical vortex may present very different patterns and using the phase average based on f_{rope} might lead to misleading conclusions. Temporal changes in the volume of the cavitating core have been observed to affect the surrounding velocity field significantly. These volume changes might be due to the self-rotation of the vortex or the result of a possible breathing mechanism. Further investigations are required to determine the key-role factor. Work is still ongoing to determine the causes of the upper part-load instability and explain the high-amplitude fluctuations as well as the elliptical shape of the cavitating vortex rope.

Acknowledgement

This research is funded by the Swiss Federal Office of Energy SFOE in the framework of the project POST under the grant agreement SI/501943-01. In addition, the authors would like to thank Nippon Koei Co., Ltd. (Japan) for making available the reduced-scale model.

References

[1] Fisher, R. K., Palde, U., Ulith, P., 1980, “Comparison of draft tube surging of homologous scale models and prototype Francis turbines,” In Proceeding of the 10th IAHR Symposium on Hydraulic Machinery and Systems (Tokyo, 1980), pp. 541-556.

[2] Dörfler, P. K., 1994, “Observation of the pressure pulsation on Francis model turbine with high specific speed,” Hydropower & Dams (January 1994), 21-26.

[3] Nicolet, C., Zobeiri, A., Maruzewski, P. and Avellan, F., 2010, August. On the upper part load vortex rope in Francis turbine: Experimental investigation. In IOP Conference Series: Earth and Environmental Science (Vol. 12, No. 1, p. 012053). IOP Publishing.

[4] Koutnik, J., Krüger, K., Pochyly, F., Rudolf, P. and Haban, V., 2006, June. On cavitating vortex rope form stability during Francis turbine part load operation. In Proceedings of the first Meeting of the IAHR Int. Working Group on Cavitation and Dynamic Problems in Hydraulic Machinery and Systems (Barcelona (Vol. 304).

[5] Kirschner, O., Ruprecht, A. and Göde, E., 2009, October. Experimental investigation of pressure pulsation in a simplified draft tube. In Proceedings of the 3rd IAHR International Meeting of the Workgroup on Cavitation and Dynamic Problems in Hydraulic Machinery and Systems, Brno, Czech Republic (pp. 55-65).

[6] Favrel, A., Liu, Z., Takahashi, W., Irie, T., Kubo, M. and Miyagawa, K., 2019, December. Visualization of the elliptical form of a cavitation vortex rope and its collapse by two cameras. In IOP Conference Series: Earth and Environmental Science (Vol. 405, No. 1, p. 012035). IOP Publishing.